

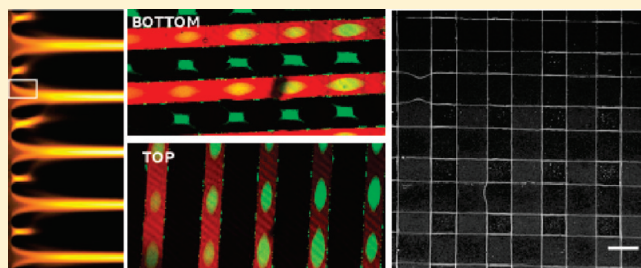
Dynamic Templating of Colloidal Patterns in Three Dimensions with Nonuniform Electric Fields

Andrew P. Bartlett,[†] Amit K. Agarwal,[‡] and Anand Yethiraj^{*}

Department of Physics and Physical Oceanography, Memorial University, St. John's, Newfoundland and Labrador, Canada A1B 3X7

S Supporting Information

ABSTRACT: Order–disorder transitions in colloidal systems are an attractive option for making switchable materials. Electric-field-driven order–disorder transitions are especially attractive for this purpose because the tuning parameter is easily and externally controllable. However, precise positional control of 3D structure is immensely challenging. Using patterned electrodes, we demonstrate that ac electric fields—dominantly dielectrophoresis (DEP) coupled with an electrohydrodynamic mechanism consisting of induced-charge electro-osmosis (ICEO)—can be used to template colloidal order dynamically in three dimensions. We find that the electric field geometry dictates the location, size, and shape of colloidal patterns and can produce patterns with surprising complexity.



dictates the location, size, and shape of colloidal patterns and can produce patterns with surprising complexity.

INTRODUCTION

Colloidal order–disorder transitions offer unique opportunities for reversibly assembling and disassembling 2D and 3D structures on the micrometer and nanometer scales.^{1–6} The length scale of these colloidal structures is chosen by the self-assembling system itself and is not easily tunable. New kinds of hybrid composite materials comprising more open cellular colloidal structures have been created.^{7–10} These provide access to structural length scales other than the intrinsic lattice periodicity, and such open structures can combine lightness with structural strength. Another method of creating lower-dimensional structures, such as nanowires,¹¹ is the introduction of anisotropy.¹² Electric-field-tunable colloids exhibit a rich diversity of stable equilibrium 3D structures^{6,13,14} that can be switched on by anisotropic dipolar forces,¹⁵ that are also important for nanoparticle self-assembly^{11,16,17} as well as stable nonequilibrium 2D structures based on electrohydrodynamic forces (EHD).^{18,19}

However, controlling both the structural length scale and the precise location of colloidal structures requires some form of surface templating.^{20,21} Combining electric fields with surface templating provides the opportunity to control patterns dynamically. Dipolar interactions induced by an external electric field have competing angle-dependent attractive and repulsive contributions that have frustrated past attempts at surface templating. Dielectrophoretic (DEP) forces, achieved using electrodes patterned on micrometer to millimeter scales,²² have been previously used both to separate²⁴ and to concentrate particle species.²⁵ In addition, the ability to control particle locations using DEP,^{26,27} EHD,²⁸ and a combination of DEP and EHD²⁹ in one and two dimensions has been demonstrated. Finally, induced-charge electro-osmosis (ICEO)^{30,31} and electrothermal flows^{32,33} have been shown to produce measurable flows with ac

electric fields in microelectrode geometries at low and high frequencies, respectively.

In this work, we demonstrate the dynamic templating of colloidal patterns with 3D control and long-range order using 3D electric fields generated by electrodes patterned on the micrometer scale. We show control over the location, size, and shape of colloidal structure over large areas (several millimeters) via control of the electrode geometry. In particular, the size of the patterned feature is controllable on length scales smaller than the electrode width. By varying the frequency, we find a qualitative change in the nature of stable patterns, signaling a crossover from a DEP-dominant regime to a regime where EHD is also important. As far as we know, such control has not been demonstrated previously.

EXPERIMENTAL SECTION

The patterned plate electrodes were fabricated on 20 × 20 mm microscope cover slides coated with indium tin oxide (ITO) (Structure Probe Inc., 30–60 Ω/sq). A layer of Shipley S 1813 photoresist was spin coated onto the plates for 30 s at 4000 rpm, followed by a 1 min soft bake. The substrate was then exposed to an ultraviolet exposure pattern using a maskless patterning system (Intelligent Micro Patterning SF 100). The pattern was developed by submerging the substrate in a 1% (w/v) solution of NaOH for several seconds. The exposed ITO pattern was then etched by submerging the substrate in HCl (11.65 M) for 30 s.

Wire leads were soldered onto sections of paper clips for structural strength and glued to the substrate (using NOA 63 UV curing epoxy). Electrical contact between the conducting layer and the wire lead was

Received: January 17, 2011

Revised: March 10, 2011

Published: March 18, 2011

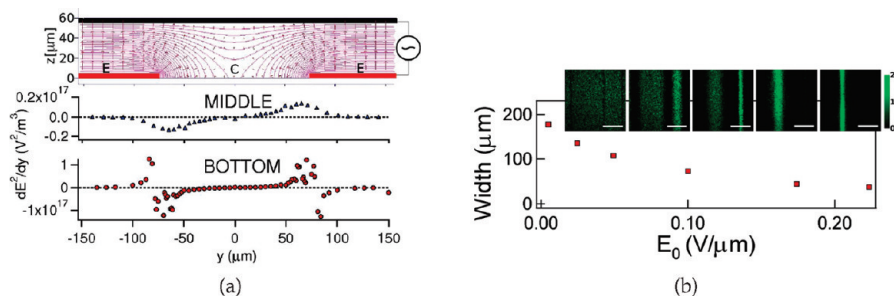


Figure 1. Bottom-stripe geometry. (a) Two-dimensional z – y cut of 2D electric equipotentials and field vectors within a bottom-stripe cell (top) and profiles of the gradient of the field intensity (∇E^2) vs position near the middle and at the bottom plate. (b) Width of the particle-rich region decreases with the applied field strength. Images constructed by summing all slices taken at different heights z from a 3D image stack, left to right: $V_{pp} = 0.77, 3.8, 7.6, 15.4, 34.4$ V. Scale bar = $100 \mu\text{m}$. $f = 100$ kHz, sample thickness = $77 \mu\text{m}$, $\phi \approx 0.4\%$, and $\sigma = 0.8 \mu\text{m}$.

made using silver paste. The electrical leads were connected to an amplifier (Krohn-Hite Corp., model 7602M), which receives its input signal from a function generator (Tektronix AFG 3022). Electric field visualizations in 2D and 3D were produced using commercial software packages (Poisson SuperFish and Maxwell3D).

The sample cells were then constructed by gluing the bottom plate electrode (conducting side up) to a glass microscope slide. Two $50 \mu\text{m}$ spacers were placed on top of the electrode such that the area of interest was between the spacers. The top electrode was then placed on top of the spacers (conducting side down) and attached with UV curing glue in a manner that left an opening on two sides of the sample. The sample was filled by placing a drop of colloidal suspension on one of the open ends, and UV glue was used again to seal two open ends (with the sample area covered to prevent bleaching).

The aqueous colloidal suspension consists of a $0.8\text{-}\mu\text{m}$ -diameter (FITC-labeled, blue excitation and green emission) fluorescent core and nonfluorescent-shell silica particles suspended in a refractive-index-matching solution of dimethyl sulfoxide and water (85:15 v/v).³⁷ The sample was imaged with a Nikon Eclipse 80-i microscope equipped with a Qimaging QICAM Fast 1394 monochrome digital camera. The nonaqueous colloidal suspensions were 0.8- and $1.0\text{-}\mu\text{m}$ -diameter fluorescently labeled PMMA particles suspended in a tetrachloroethylene–decalin (40:60 v/v) solvent mixture. The electrode/particles were imaged using laser confocal reflection/fluorescence scanning microscopy.

RESULTS AND DISCUSSION

We focus on experimental results using two electrode geometries. In the “bottom-stripe” geometry, the top ITO-coated glass surface is connected to ground and the bottom patterned ITO substrate is connected to an ac signal. Electric potentials and field lines obtained from simulations are shown in Figure 1a (when the bottom electrode is at $+V_{pp}$). The dielectrophoretic force on a colloidal sphere²² is $F_{DEP} = \pi R^3 \epsilon_m K \nabla E^2$, where R is the particle diameter, K is the real part of the Clausius–Mosotti factor ($K \approx -0.4$ for silica in water–DMSO), $\epsilon_m \approx 50\epsilon_0$ is the medium permittivity, and $E = (2)^{1/2} E_{rms}$ is the zero-peak electric field. Figure 1a shows that the value of ∇E^2 near the bottom electrode and thus the magnitude of F_{DEP} are largest in the vicinity of the electrode edge, and the sign of the force changes across it. Further up, F_{DEP} is always facing inward toward the center (for $K < 0$). Finally, there is a region of zero force in between electrode edges in positions labeled “C” (the central minimum in the gap between the electrodes) and “E” (at the center of each electrode) in Figure 1a. In suspensions where $K < 0$ (true for most aqueous suspensions) we thus expect “negative DEP”. For $K > 0$ (realizable in many nonaqueous suspensions), one expects positive DEP

with particles moving to the electrode edge (away from positions C and E).

When the field is turned on, the particles move in the direction of the local force (the real-time dynamics is shown in Supporting Information 1, Movie 1). At each field strength, there is a stationary state. Local 2D structure in a similar system and geometry have been demonstrated previously.²³ Here, 2D images obtained by summing all slices of 3D images of such stationary states are shown for selected applied voltages in Figure 1b. The interface between the particle-rich and particle-poor region is sharp. We define for convenience $E_0 = V_{pp}/2d$, where $d = 77 \mu\text{m}$ is the sample thickness: the actual electric field is nonuniform and is significantly higher than E_0 at the electrode edge and lower in between the electrodes (regions C), but it is close to this value at the electrode center (regions E). From the 3D images, the particle density profile was peaked at the midpoints between electrode edges and well fit to a Gaussian above $E_0 \approx 0.07 \text{ V}/\mu\text{m}$: the width of the particle-rich region was found to be a decreasing function of the amplitude of the DEP force (Figure 1b).

The second geometry used was a “crossed-field” geometry, where the top plate is also a patterned ITO electrode and is positioned at an angle with respect to the bottom stripe. (Here the angle is close to 90° .) We find that this field geometry is complex enough to yield a long-range (and centimeter-scale) positioning of particles in regions in between the electrode edges. (In Figure 2a, electrodes are red and particle-rich regions are green.) The particulate regions are not only on the substrates but have a 3D extent (Figure 2b). This can be seen in the x – z and y – z cuts (bottom and right) as well as in the inset, which shows an exponential decrease in intensity versus height with a characteristic length of $3.8 \pm 0.1 \mu\text{m}$.

We focus first on the dynamics of particle assembly in the bottom-stripe geometry (Figure 1a). Time-resolved microscopy of $0.8\text{-}\mu\text{m}$ -diameter silica spheres in an aqueous suspension in the bottom-stripe geometry (Figure 3) shows the emergence of regions of high particle density in regions of zero force soon after an electric field is turned on. However, the global minimum in field strength between the electrodes (regions C) is a stable point, and the region in the center of the electrode (regions E) is unstable to perturbations. The reason for this (as shown in Figure 1a) is that colloidal particles that are some distance z above the bottom electrode experience a force toward the center at all (x, y) positions. From the dynamics of field-induced segregation, we obtain the relation between the velocity of particle fronts and ∇E^2 . This is done as follows. The front position

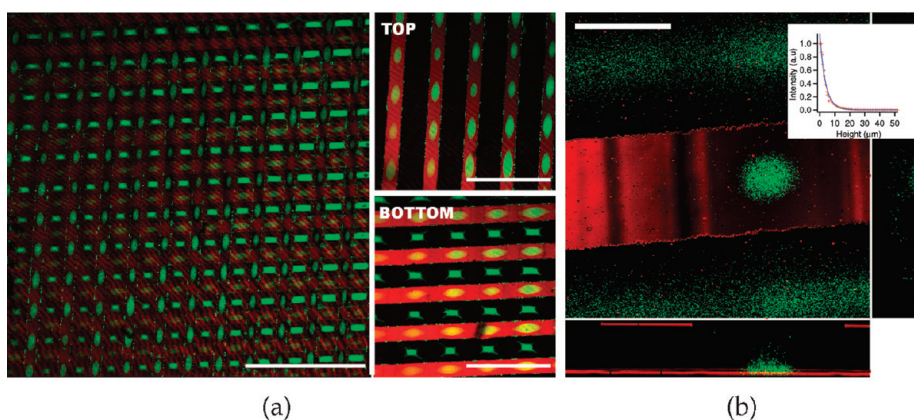


Figure 2. Crossed-field geometry. (a) Long-range order. (Left) Selected area from a centimeter-scale pattern of $250 \mu\text{m}$ periodicity and $62 \mu\text{m}$ sample thickness ($V_{\text{pp}} = 40.8 \text{ V}$, $f = 10 \text{ kHz}$, scale bar 1 mm). (Right:) Colloids (green) are seen in two sets of regions: below the top and above the bottom electrodes (in red) and in between electrodes. Scale bar = 0.5 mm . (b) Particle-rich regions occur in between electrode edges and have controllable shape and size as well as a 3D extent (as shown in the bottom and side panels and an exponentially decaying intensity profile in the inset). $\phi \approx 0.4\%$, $V_{\text{pp}} = 20.4 \text{ V}$, $f = 100 \text{ kHz}$, scale bar = $50 \mu\text{m}$.

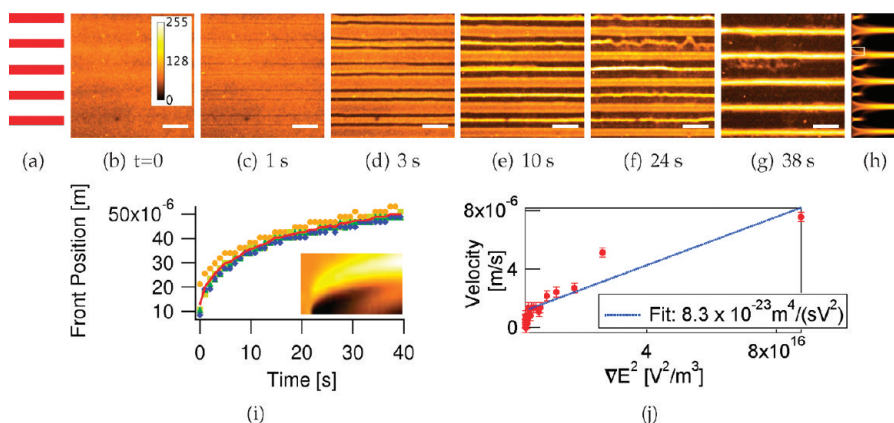


Figure 3. Dynamics in bottom-stripe geometry. (a) Schematic of the bottom electrode (red). (b–g) Time series of y – x fluorescence micrographs ($4\times$ objective) of colloidal particles after an electric field is turned on ($t = 0$). Scale bar = $200 \mu\text{m}$. $V_{\text{pp}} = 30 \text{ V}$, $f = 100 \text{ kHz}$, sample thickness = $60 \mu\text{m}$, $\phi \approx 0.4\%$. (h) Position timeline (y – t) for the particulate front: each column of unit pixel width is the intensity averaged over x for one frame in the time series. (i) Dynamics of the particulate front. Each timeline (obtained from a different stripe) is represented by a differently colored symbol. The solid red line is the average of all timelines. (Inset) The highlighted section of part h (inverted) is a sample of the source data for the timelines. (j) Velocity vs ∇E^2 . For larger ∇E^2 , a linear fit is consistent with a DEP mechanism.

timeline (Figure 3h) is extracted from the image time series shown in Figure 3b–g. (The entire movie is included in Supporting Information 1, Movie 1). The front position versus time is extracted from each of these timelines (Figure 3i, one such timeline is shown, inverted, in the inset). Viscosity dominates at low Reynolds number; therefore, the particle velocity v at any instant obtained from Figure 3i is governed by an instantaneous balance of viscous and applied forces. Assuming that only the dielectrophoretic force is important, we plot v versus ∇E^2 in Figure 3j. The relationship for large ∇E^2 is roughly linear. The viscous force is given by $F_{\text{visc}} = \xi v$, where for an isolated spherical particle $\xi = 6\pi\eta R$. Force balance yields a relationship for the velocity: $v = \mu_{\text{DEP}} \nabla E^2$ where $\mu_{\text{DEP}} = (\pi R^3 \epsilon_m K) / \xi$. Shown in Figure 3j is a linear fit that yields a slope of $\mu_{\text{DEP}} = 8.3 \times 10^{-23} \text{ m}^4 / (\text{s V}^2)$ and an intercept of $v_0 = 1.0 \pm 0.2 \mu\text{m/s}$. The slope implies that $\xi \approx 4 \times 10^{-7} \text{ N s/m}$, which is an order of magnitude larger than the Stokes drag for an isolated sphere in free solution; this is reasonable for particle-rich regions close to a surface. The local slope yields μ_{DEP} that increases with time (i.e., with

decreasing ∇E^2). This is qualitatively consistent with simulations that find a dielectrophoretic mobility that increases with time due to either the coupling of particle and solvent motions or dimer formation.³⁴ Another possible mechanism contributing to flow is ac electro-osmosis (ICEO).^{30,31} Supporting the existence of ICEO is the observation is that particulate agglomeration is more rapid in the unstable region above the electrodes. Particulate flow in this region is likely enhanced by ICEO, which would be directed away from both the electrode edge and the gap. The importance of this electro-osmotic flow is clearer in experiments in the crossed-field geometry, as discussed next.

For the crossed-field geometry, we find that the steady-state structures are a function of both field magnitude and frequency. The frequency and field amplitude dependence of the structure formation is shown in Figure 4, which shows (left and middle) confocal micrographs with a $40\times$ objective of top and bottom plates, respectively; particles are in green, and electrodes are red. On the right are fluorescence micrographs of the same region

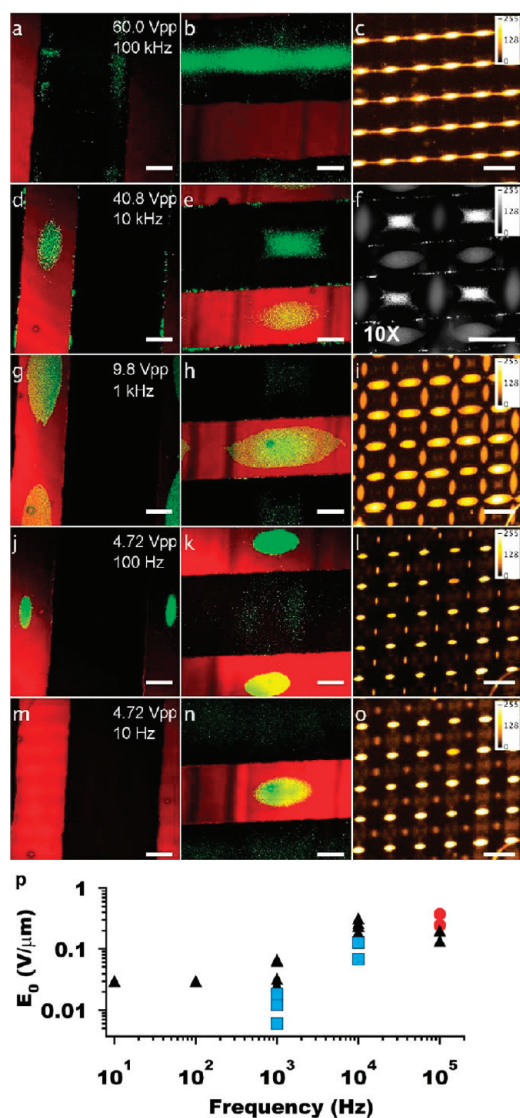


Figure 4. Field and frequency control of patterns in crossed-field geometry. $\phi \approx 0.4\%$ and $\sigma = 0.8 \mu\text{m}$. Sample thickness = $88.7 \mu\text{m}$, so a peak–peak voltage of $5V_{pp}$ corresponds to a field (far from the electrode edges) of $E_0 = 0.06 \text{ V}/\mu\text{m}$. (a–o) Columns 1 and 2: confocal micrograph ($40\times$, NA = 0.600 objective) of top and bottom plates. Green/red represents particles/electrodes. Scale bar = $50 \mu\text{m}$. Column 3: fluorescence micrograph ($4\times$, unless otherwise shown). The potential and field frequency applied across the cell are shown in the first column. Scale bar = $200 \mu\text{m}$. (p) Nature of patterns as a function of field and frequency. Red circles: particles only between electrodes. Blue squares: particles only above or below electrodes. Black triangles: particles in all of the above locations. For a discussion, see the text.

with lower-magnification objectives. At 100 kHz, we initially see a similar process to that in the previous case (shown in Supporting Information 2, Movie 2). The particles are all at the bottom to begin with and recede away from the bottom-electrode edges. However, in this case the top electrodes provide a (periodic) pathway for the particles in the metastable minima (regions E, located near the bottom-electrode center) to flow to the stable minima (regions C). The final state has no agglomeration of particles at the top plate (Figure 4a) and a striped agglomeration pattern between the electrodes near the bottom plate (Figure 4b).

The salient difference in the final state is that the stripes have a modulated intensity (Figure 4c).

The location of the particle agglomeration can be controlled with frequency. At frequencies of 10 kHz and lower, one observes two distinct types of patterns (Figure 4d,e,g,h,j,k,n): “rectangles” that occur in the electrode gap and “eyes” that occur above or below the bottom or top electrode and between the electrode edges. Compared with the 3D electric field simulation of the crossed-field geometry (shown in Supporting Information 3, Figure 1), we see that the rectangular particulate regions are indeed above the minimum in between the electrodes and that the eyes (either above the bottom or below the top electrode) represent regions that have a low $|\nabla E^2|$ but with a force (for $K < 0$) that points away from the electrode, thus not a stable minimum.

There are three distinct locations of particle agglomeration: eyes below the top electrode but between the bottom electrodes (Figure 4a,d,g,j,l), eyes above the bottom electrode but in between the top electrodes, and rectangles in the electrode gap between the bottom electrodes (Figure 4b,e,h,k,n). If the patterns were driven purely by DEP, then one would only see the rectangular patterns in the stable minimum in the electrode gap (with the bottom of the gap being favored by gravitational forces). This is indeed the high-frequency structure. The presence of the eye-shaped patterns at lower frequencies could arise from electrohydrodynamic flows. As discussed in the bottom-stripe geometry, ac electrohydrodynamics arising from induced-charge electro-osmosis (ICEO)^{29–31,35} gives rise to flows away from the electrode edges and toward the center of the electrode. These flows would account for the nonzero particle speeds at low $|\nabla E^2|$, frequencies lower than 1 MHz in Figure 3j, and the stabilization of the eyes in Figure 4. Other possibilities for electric-field-driven fluid flow, such as electrothermal effects,^{32,33} are more dominant at frequencies above 1 MHz.

A phase diagram summarizes the behavior (Figure 4p). At high frequencies (100 kHz, here ICEO should be least important), particles are all in the (rectangular) minimum. At low frequencies (where ICEO is most relevant), we observed particles only in the “eyes”. At intermediate frequencies, mixed patterns with quantitatively different populations in the rectangles and eyes are observed. See Supporting Information 5, Figure 2 for more details. The existence of mixed patterns allows us to rule out switching from positive to negative DEP, which in any case is not expected for silica colloids in aqueous solution.²⁷ In addition, we do detect the slow exchange of particles between the rectangles and the eyes. The broad (10 Hz–100 kHz) frequency range of this phenomenon confirms an electrohydrodynamic mechanism for the stabilization of the DEP-metastable regions.²⁹ Whereas both ICEO and DEP velocities are frequency-dependent, ICEO speeds depend globally on E_0^2 (where E_0 is the applied electric field)³¹ and DEP speeds depend on $|\nabla E^2|$ (where E is the local electric field): the relative importance is observed to be tunable with field and frequency.

Finally, we show that upon inverting the dielectric constant mismatch (PMMA colloids in a nonaqueous solvent) one can obtain pure DEP. Positive DEP has been demonstrated in different colloidal systems.^{24,25} We show that in sample geometries identical to those used in the aqueous suspensions, particles migrate toward the electrode edges (Figure 5a shows $0.8 \mu\text{m}$ colloids at $\phi \approx 1\%$), and there is no electro-osmotic flow away from the electrode edges even at low frequencies. In addition, we see that at much higher concentrations (Figure 5b–d shows $1.0 \mu\text{m}$ colloids at $\phi \approx 15\%$) the osmotic pressure is high enough

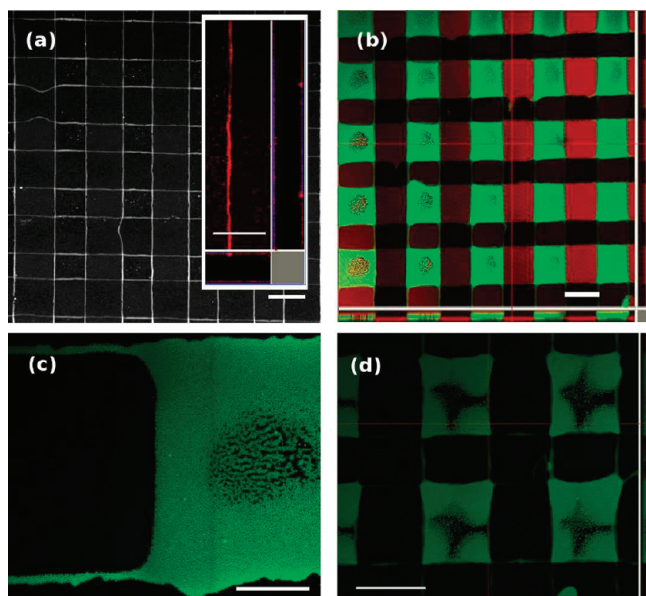


Figure 5. Positive dielectrophoresis and dipolar structures in nonaqueous colloidal suspensions at low and high particle concentrations. (a) 0.8- μm -diameter particles, $E_0 = 2.8 \text{ V}/\mu\text{m}$, $\phi \approx 1\%$, scale bar = 150 μm . Particles agglomerate at electrode edges. Inset (scale bar 50 μm) shows a confocal image of x - y , x - z , and y - z cuts of a 3D image that shows that the particle aggregation is within micrometers of the substrate. (b) Structures at higher concentrations, 1.0- μm -diameter particles. $E_0 = 1.4 \text{ V}/\mu\text{m}$, $\phi \approx 15\%$, scale bar = 150 μm . Particles (green) collect both at electrode edges (red) and in regions of high electric field. (c) $E_0 = 2.0 \text{ V}/\mu\text{m}$, $\phi \approx 15\%$, scale bar = 50 μm . In a region in between two electrodes, where the field is most uniform, dipolar structures are observed. (d) $E_0 = 2.7 \text{ V}/\mu\text{m}$, $\phi \approx 15\%$, scale bar = 150 μm . At higher fields, the particles in between electrodes are forced increasingly toward the region of highest ∇E^2 .

that particles do not all reside at electrode edges. In this instance, particles are also found in regions of high electric field (where the top and bottom electrodes overlap in x - y). Here, we also see the expected dipolar order, described elsewhere,¹³ but the particles increasingly migrate toward the edges with increasing field strength (Figure 5b–d). A 3D stack of the order near the bottom plate (Figure 5c) (shown in Supporting Information 4, Movie 3) shows that the particle structures extend about 6.5 μm in the z direction. This happens at both electrodes.

Whereas the pattern-forming dynamics is slow for millisecond-scale display applications, the front speeds can be increased by employing geometries where the field nonuniformities are larger. For example, the dynamics at a bottom-patterned electrode with square holes, shown in Supporting Information 6, Figure 3 is more rapid. Moreover, intricate control of the 3D location, shape, and size of particulate patterns and the possibility of very low control voltages (as low as 5 V, Figure 4j–o) could be very useful for slower switching applications, for example, in microchannels or for electronic paper. In addition, these patterns can be made permanent by previously established methods³⁶ via slow polymerization. They could also be used as dynamically switchable cells for parallelizable reactions or processes controlled by particle concentration (cf. Figure 4c,f,i,l,o or Supporting Information 6, Figure 3) with even the possibility to have cells with simultaneous multiple length scales and to control particle concentrations in three dimensions.

CONCLUSIONS

In this study, we have demonstrated precise micrometer-scale positional control of colloidal structure with patterned ac electric fields over sample areas of several millimeters. An increase in the complexity of the electric field geometry results in 3D structures with controllable shape and size. We demonstrate pattern selectivity as a function of field frequency. At high frequencies, dielectrophoresis (DEP) dominates and ac electro-osmosis is increasingly important as the frequency is lowered. The control achieved here could be easily adapted to microfluidic applications, for example, in switching (on or off) reactions controlled by particle concentrations and for display applications.

ASSOCIATED CONTENT

S Supporting Information. A y - z cut of the ∇E^2 vector field. Field dependence of particulate patterns at different frequencies. Patterned ITO substrate consisting of square ITO-free regions. Movies showing the transient dynamics after the ac electric field ($f = 100 \text{ kHz}$) is turned on in the bottom-stripe and crossed-field geometries and a 3D scan of the colloidal structure near the bottom electrode in a nonaqueous suspension that exhibits positive DEP. This material is available free of charge via the Internet at <http://pubs.acs.org>.

AUTHOR INFORMATION

Corresponding Author

*E-mail: ayethiraj@mun.ca.

Present Addresses

[†]Department of Physics and Astronomy, McMaster University, Hamilton, Ontario, Canada L8S 4M1.

[‡]Instruments Research and Development Establishment, Raipur Road, Dehradun, India 248008

ACKNOWLEDGMENT

We gratefully acknowledge Erika Merschrod (Chemistry, Memorial) for the use of the maskless patterning system, Robert Cove (Engineering, Memorial) for providing visualizations of 3D electric field profiles, and Mikko Karttunen for some insightful comments. This work was supported by the NSERC.

REFERENCES

- (1) Pusey, P. N.; van Megen, W. Phase-behavior of concentrated suspensions of nearly hard colloidal spheres. *Nature* **1986**, 320, 340.
- (2) Lowen, H. Melting, freezing and colloidal suspensions. *Phys. Rep.* **1994**, 237, 249.
- (3) Gast, A. P.; Russel, W. B. Simple ordering in complex fluids. *Phys. Today* **1998**, 51, 24.
- (4) van Blaaderen, A. Colloids under external control. *MRS Bull.* **2004**, 29, 85.
- (5) Shevchenko, E. V.; Talapin, D. V.; Kotov, N. A.; O'Brien, S.; Murray, C. B. Structural diversity in binary nanoparticle superlattices. *Nature* **2006**, 439, 55.
- (6) Yethiraj, A. Tunable colloids: control of colloidal phase transitions with tunable interactions. *Soft Matter* **2007**, 3, 1099.
- (7) Deville, S.; Saiz, E.; Nalla, R. K.; Tomsia, A. P. Freezing as a path to build complex composites. *Science* **2006**, 311, 515.
- (8) Munch, E.; Launey, M. E.; Alsem, D. H.; Saiz, E.; Tomsia, A. P.; Ritchie, R. O. Tough, bio-inspired hybrid materials. *Science* **2008**, 322, 1516.

- (9) Velev, O. D.; Kaler, E. W. Structured porous materials via colloidal crystal templating: from inorganic oxides to metals. *Adv. Mater.* **2000**, *12*, 531.
- (10) Agarwal, A.; Yethiraj, A. Low-density ordered phase in brownian dipolar colloidal suspensions. *Phys. Rev. Lett.* **2009**, *102*, 198301.
- (11) Tang, Z.; Kotov, N. A.; Giersig, M. Spontaneous organization of single CdTe nanoparticles into luminescent nanowires. *Science* **2002**, *297*, 237.
- (12) Glotzer, S. C.; Solomon, M. J. Anisotropy of building blocks and their assembly into complex structures. *Nat. Mater.* **2007**, *6*, 557.
- (13) Yethiraj, A.; van Blaaderen, A. A colloidal model system with an interaction tunable from hard sphere to soft and dipolar. *Nature* **2003**, *21*, 513.
- (14) Leunissen, M. E.; Vutukuri, H. R.; van Blaaderen, A. Directing colloidal self-assembly with biaxial electric fields. *Adv. Mater.* **2009**, *21*, 3116.
- (15) Parthasarathy, M.; Klingenberg, D. J. Electrorheology: mechanisms and models. *Mater. Sci. Eng., R* **1996**, *17*, 57.
- (16) Min, Y.; Akbulut, M.; Kristiansen, K.; Golan, Y.; Israelachvili, J. The role of interparticle and external forces in nanoparticle assembly. *Nat. Mater.* **2008**, *7*, 527.
- (17) Richardi, J.; Pileni, M. P.; Weis, J.-J. Self-organization of magnetic nanoparticles: A Monte Carlo study. *Phys. Rev. E* **2008**, *77*, 061510.
- (18) Trau, M.; Saville, D. A.; Aksay, I. A. Field-induced layering of colloidal crystals. *Science* **1996**, *272*, 706.
- (19) Zhang, K.-Q.; Liu, X. Y. Controlled formation of colloidal structures by an alternating electric field and its mechanisms. *J. Chem. Phys.* **2009**, *130*, 184901.
- (20) Hoogenboom, J. P.; Retif, C.; de Bres, E.; van de Boer, M.; van Langen-Suurling, A. K.; Romijn, J.; van Blaaderen, A. Template-induced growth of close-packed and non-close-packed colloidal crystals during solvent evaporation. *Nano Lett.* **2004**, *4*, 205.
- (21) Ofir, Y.; Moran, I. W.; Subramani, C.; Carter, K. R.; Rotello, V. M. Nanoimprint lithography for functional three-dimensional patterns. *Adv. Mater.* **2010**, *22*, 3608.
- (22) Pohl, H. A. *Dielectrophoresis: The Behavior of Neutral Matter in Nonuniform Electric Fields*; Cambridge Monographs on Physics; Cambridge University Press: Cambridge, U.K., 1978.
- (23) Juarez, J. J.; Bevan, M. A. Interactions and microstructures in electric field mediated colloidal assembly. *J. Chem. Phys.* **2009**, *131*, 134704.
- (24) Krupke, R.; Hennrich, F.; Lohneysen, H. v.; Kappes, M. M. Separation of metallic from semiconducting single-walled carbon nanotubes. *Science* **2003**, *301*, 344.
- (25) Sullivan, M. T.; Zhao, K.; Hollingsworth, A. D.; Austin, R. H.; Russel, W. B.; Chaikin, P. M. An electric bottle for colloids. *Phys. Rev. Lett.* **2006**, *96*, 015703.
- (26) Arnold, W. M. Particle patterning using fluidics and electric fields. *IEEE Trans. Dielectr. Electr. Insul.* **2008**, *15*, 144.
- (27) Docoslis, A.; Alexandridis, P. One, two, and three-dimensional organization of colloidal particles using nonuniform alternating current electric fields. *Electrophoresis* **2002**, *23*, 2174.
- (28) Xie, R.; Liu, X. Y. Electrically directed on-chip reversible patterning of two-dimensional tunable colloidal structures. *Adv. Funct. Mater.* **2008**, *18*, 802.
- (29) Green, N. G.; Morgan, H. Separation of submicrometre particles using a combination of dielectrophoretic and electrohydrodynamic forces. *J. Phys. D: Appl. Phys.* **1998**, *31*, L25.
- (30) Ramos, A.; Morgan, H.; Green, N. G.; Castellanos, A. ac electric-field-induced fluid flow in microelectrodes. *J. Colloid Interface Sci.* **1999**, *217*, 420.
- (31) Bazant, M. A.; Squires, T. M. Induced-charge electrokinetic phenomena: theory and microfluidic applications. *Phys. Rev. Lett.* **2004**, *92*, 066101.
- (32) Burg, B. R.; Schneider, J.; Maurer, S.; Schirmer, N. C.; Poulikakos, D. Electrokinetic framework of dielectrophoretic deposition devices. *J. Appl. Phys.* **2010**, *107*, 124308.
- (33) Burg, B. R.; Schneider, J.; Bianco, V.; Schirmer, N. C.; Poulikakos, D. Selective parallel integration of individual metallic single-walled carbon nanotubes from heterogeneous solutions. *Langmuir* **2010**, *26*, 10419.
- (34) Salonen, E.; Terama, E.; Vattulainen, I.; Karttunen, M. Dielectrophoresis of nanocolloids: a molecular dynamics study. *Eur. Phys. J. E* **2005**, *18*, 133. Salonen, E.; Terama, E.; Vattulainen, I.; Karttunen, M. Enhanced dielectrophoresis of nanocolloids by dimer formation. *Europhys. Lett.* **2007**, *78*, 48004.
- (35) Hoettges, K. F.; McDonnell, M. B.; Hughes, M. P. Use of combined dielectrophoretic/electrohydrodynamic forces for biosensor enhancement. *J. Phys. D: Appl. Phys.* **2003**, *36*, L101.
- (36) Yethiraj, A.; Thijssen, J.; Wouterse, A.; van Blaaderen, A. Large electric-field-induced colloidal single crystals for photonic applications. *Adv. Mater.* **2004**, *16*, 596.
- (37) Li, N.; Newman, H.; Valera, M.; Saika-Voivod, I.; Yethiraj, A. Colloids with a tunable dipolar interaction: equations of state and order parameters via confocal microscopy. *Soft Matter* **2010**, *6*, 876.